Astron. Astrophys. 352, 297–307 (1999)

ASTRONOMY AND ASTROPHYSICS

The dust content of planetary nebulae: a reappraisal*

Grażyna Stasińska[1] **and Ryszard Szczerba**[2]

[1] DAEC, Observatoire de Paris-Meudon, 92195 Meudon Cedex, France (grazyna@obspm.fr)
[2] N. Copernicus Astronomical Center, Rabiańska 8, 87-100 Toruń, Poland (szczerba@ncac.torun.pl)

Received 2 June 1999 / Accepted 4 October 1999

Abstract. We have performed a statistical analysis using broad band IRAS data on about 500 planetary nebulae with the aim of characterizing their dust content. Our approach is different from previous studies in that it uses an extensive grid of photoionization models to test the methods for deriving the dust temperature, the dust-to-gas mass ratio and the average grain size. In addition, we use only distance independent diagrams.

With our models, we show the effect of contamination by atomic lines in the broad band IRAS fluxes during planetary nebula evolution. We find that planetary nebulae with very different dust-to-gas mass ratios exist, so that the dust content is a primordial parameter for the interpretation of far infrared data of planetary nebulae. In contrast with previous studies, we find no evidence for a decrease in the dust-to-gas mass ratio as the planetary nebulae evolve. We also show that the decrease in grain size advocated by Natta & Panagia (1981) and Lenzuni et al. (1989) is an artefact of their method of analysis. Our results suggest that the timescale for destruction of dust grains in planetary nebulae is larger than their lifetime.

Key words: ISM: planetary nebulae: general – infrared: stars – stars: AGB and post-AGB – stars: circumstellar matter – radiative transfer

1. Introduction

Far infrared measurements of planetary nebulae allow one to investigate their dust content. From broad band photometry, one can derive the characteristic temperature of the emitting dust and the total amount of energy that it radiates.

For example, Natta & Panagia (1981), using the aircraft observations by Moseley (1980), analyzed a sample of 10 planetary nebulae, and found evidence that the dust-to-gas mass ratio, $m_{\rm d}/m_{\rm g}$, and the grain size were decreasing systematically with nebular radius, indicating a time variation of the dust properties in planetary nebulae. Then, Pottasch et al. (1984a) used IRAS broad band photometry to analyze a sample of 46 planetary nebulae. They also found $m_{\rm d}/m_{\rm g}$ to decrease with radius, being as large as a few 10^{-2} for the smallest nebulae and two order of magnitudes smaller for the largest ones. Later, Lenzuni et al. (1989) repeated the analysis of Natta & Panagia (1981) on a much larger sample: they analyzed 233 planetary nebulae which had been observed by IRAS in at least the 25 μm and 60 μm bands and appeared in the Daub (1982) catalog of distances. Essentially, they confirmed the finding of Natta & Panagia (1981).

The problem of the infrared luminosity of planetary nebulae has been addressed by several authors: Pottasch et al. (1984a), Iyengar (1986), Zijlstra et al. (1989), Ratag et al. (1990), Amnuel (1994). Pottasch et al. (1984a) found that very high infrared excesses (IRE, i.e. the infrared luminosity in terms of what can be accounted for by absorption of the Lyα radiation produced in the nebula) were usually found in the small, high dust temperature nebulae. They concluded that, in these cases, dust is probably mostly heated by the radiation of the central star on the longwave side of Lyα, since the nebulae are young. Ratag et al. (1990) also considered the possibility that high IRE could be due to high dust contents or to heating by the interstellar radiation field. Amnuel (1994) favored the latter explanation.

All the studies above based their conclusions either on a simple, empirical interpretation of the data, or, in the best cases, on semi-analytical models of planetary nebulae that involve drastic simplifications. Also, excepting the studies specifically devoted to planetary nebulae in the Galactic bulge (Ratag et al. 1990), they rely heavily on the adopted distances to the nebulae. Therefore, they must be considered with caution. A safer approach, in our opinion, for studies of statistical nature, is to interpret the observed data with the help of grids of numerical models that are able to compute the observables and use distance independent diagrams. Such an approach for the interpretation of the infrared emission of planetary nebulae has been attempted by Volk (1992) and Vil'koviskii & Efimov (1992). Unfortunately, both these studies were rather exploratory, and did not address explicitly the questions mentioned above.

Fifteen years after the publication of the results of the IRAS mission, there is still work to be done on their interpretation as regards the statistical dust properties of planetary nebulae. It is the purpose of the present paper to contribute to this, by analyzing the broad band IRAS fluxes of planetary nebulae in the light

Send offprint requests to: Grażyna Stasińska (grazyna@obspm.fr)

* Table 1 is only accessible in electronic form at the CDS via anonymous ftp to cdsarc.u-strasbg.fr (130.79.128.5) or via http://cdsweb.u-strasbg.fr/Abstract.html

of series of dusty photoionization models for evolving planetary nebulae using distance independent diagrams. In Sect. 2, we briefly present the observational material. In Sect. 3, we describe the photoionization models. In Sect. 4, we analyze the contamination of IRAS broad band fluxes by line emission. In Sect. 5, we discuss the dust temperature. Sect. 6 is devoted to the dust-to-gas mass ratio, Sect. 7 to the infrared excess and Sect. 8 to the grain size. A general discussion of the main findings is given in Sect. 9.

2. The observational data base

We have considered the planetary nebulae from the Strasbourg-ESO Catalogue of Galactic Planetary Nebulae (Acker et al. 1992) that appear in the IRAS Point Source Catalog (1988) and have flux quality $Q = 3$ in at least the 25 and 60 μm bands. According to the IRAS Point Source Catalog, the error in the fluxes with $Q = 3$ is about 10 %. There are 548 such objects. The inclusion of planetary nebulae with $Q = 2$ adds only 86 objects with lower quality data, and does not change the conclusions of this paper.

Since individually determined distances in planetary nebulae are scarce and are sometimes contradictory for the same object when using different methods (e.g. Sabbadin 1986), we consider only distance-independent diagrams. We use the reddening corrected Hβ fluxes (or, equivalently, the radio fluxes at 6 cm converted into Hβ) and angular diameters from the same sources as Tylenda & Stasińska (1994). We discard data that are only upper limits. We end up with 477 nebulae for which we can compute the average surface brightness, S(Hβ), and which have the required IRAS data (i.e. 25 and 60 μm fluxes with $Q = 3$). Table 1[1] lists, in Columns 3 and 4, the adopted values of the reddening corrected Hβ fluxes and angular radii for all the nebulae having 25 and 60 μm fluxes with $Q = 3$ (Columns 1 and 2 give the planetary nebula PN G identifications and usual names, respectively). As is known, and seen from our models below, S(Hβ) is a rather robust estimator of the planetary nebula age. It is safer than the estimated planetary nebula radius, which was used in former studies on the dust-to-gas mass ratio in planetary nebulae, among other reasons, because it is distance independent.

Finally, to discuss the dust-to-gas mass ratio, we need an estimate of the gas density. We take the electron densities derived from the [S II] ratios as compiled by Górny (private communication), again discarding upper or lower limits. These densities are listed in Column 5 of Table 1. The main references are the compilation of Stanghellini & Kaler (1989), and the observations reported by Acker et al. (1989), Acker et al. (1991) and Kingsburgh & Barlow (1994). Thus, we end up with a sample of 230 objects for which we can discuss the time evolution of $m_{\rm d}/m_{\rm g}$. This sample is similar in size to the one of Lenzuni et al. (1989), but differs slightly from it because of our more restrictive conditions on the IRAS fluxes and more recent compilation of Hβ fluxes and angular diameters than Daub (1982).

[1] Table 1 is accessible in electronic form at the CDS via anonymous ftp to cdsarc.u-strasbg.fr (130.79.128.5) or via http://cdsweb.u-strasbg.fr/Abstract.html

3. The photoionization models

The modelling follows the same policy as in Stasińska et al. (1998). We construct sequences of photoionization models that represent the evolution of a nebula around a central star that has left the AGB and is progressing towards the white dwarf stage. The nebula is modelled as a uniformly expanding spherical shell of given total mass (with a relative thickness $(R_{\rm out} - R_{\rm in})/R_{\rm out} = 0.3$, where $R_{\rm in}$ and $R_{\rm out}$ are the inner and outer radius of the nebula, respectively) in which the density is supposed uniform. In such a simple representation, the parameters defining a planetary nebula are the central star mass, M_*, the nebular mass, $M_{\rm neb}$, its expansion velocity, $v_{\rm exp}$, and its chemical composition (also assumed uniform). True nebulae are, of course, more complicated than such a simple description. More elaborate dynamical models have been computed, even including departure from spherical symmetry (e.g. Frank & Mellema 1994), which aim at a better representation of the real evolution of planetary nebulae (but those models do not include dust and only a few sequences are computed). Our approach has the virtue of being sufficiently simple to allow one to run series of models covering the whole parameter space suggested by the observations and to make easier the interpretation of observational data, in the framework of general ideas on the evolution of planetary nebulae.

The models are computed with the photoionization code PHOTO, using the atomic data described in Stasińska & Leitherer (1996). The code assumes spherical geometry, with a central ionizing source. The diffuse radiation is treated assuming that all the photons are emitted outwards in a solid angle of 2π, and the transfer of the resonant photons of hydrogen and helium is computed with the same outward only approximation, but multiplying the photo-absorption cross-section by an appropriate factor to account for the increased path length due to scattering (Adams 1975). In contrast with the model planetary nebulae presented in Stasińska et al. (1998), which were aimed at discussing the emission from the ionized region only, the present models must take into account the possible presence of a neutral zone surrounding the ionized region, where dust emission also occurs. This is done by extending the computation of the radiation transfer outside the ionized zone, until the total nebular mass assigned to a given model is reached. The gas temperature is not computed in the neutral zone, but simply set to 100 K, since it has no incidence on the results presented here.

Dust is introduced as described in Harrington et al. (1988). In short, it is assumed to be composed of spherical grains with the classical size distribution ($\propto a^{-3.5}$, where a is the grain size) of Mathis et al. (1977). At each nebular radius, the equation of radiative equilibrium is solved, for 18 grain sizes logarithmically spaced between 0.005 and 0.25 μm. Dust in the models is assumed to interact only with the photons, not with the gas particles. It is heated by the attenuated stellar radiation field and

the diffuse radiation field produced in the nebula. At each radius, once the grain temperature is known for each grain size, the infrared emissivity is computed at 256 wavelengths. The total luminosity at each wavelength is calculated by integration over the nebular volume. The luminosities in the IRAS bands are obtained by convolution with the response function of the IRAS filters. As a check, the same procedure has been applied to the photoionization code written by Szczerba (see e.g. Gęsicki et al. 1996). Both codes give consistent results, and are able to reproduce the models of IC 418 and NGC 7662 by Hoare (1990).

The central stars are assumed to evolve according to the H-burning post-AGB evolutionary tracks as interpolated by Górny et al. (1997) from the tracks of Blöcker (1995) and references therein. The stars are assumed to radiate as blackbodies.

Results are presented with only one nebular abundance set (He/H = 0.084; C/H = $8.2\,10^{-5}$; N/H = $2.2\,10^{-5}$; O/H = $4.2\,10^{-4}$; Ne/H = $8.5\,10^{-5}$; Mg/H = $2.1\,10^{-5}$; Si/H = $2.2\,10^{-5}$; S/H = $1.0\,10^{-5}$; Cl/H = $1.6\,10^{-7}$; Ar/H = $3.0\,10^{-6}$; Fe/H = $2.4\,10^{-6}$), corresponding to half solar metallicity and depleted metals. In the present study, the only important effect of the gas chemical composition is to affect the energy emitted in the lines included in the IRAS bands (see below).

IRAS Low Resolution Spectroscopy of planetary nebulae (see e.g. Pottasch 1987) has shown that planetary nebulae contain several kinds of dust grains. Generally, it is believed that, in carbon rich planetary nebulae, dust is composed of carbon-based grains, e.g. graphite, anthracite, amorphous carbon and/or polycyclic aromatic hydrocarbons, while in oxygen-rich planetary nebulae it is composed of oxygen-based grains, e.g. different forms of silicates. However, observations with the Infrared Space Observatory showed that some nebulae around Wolf-Rayet central stars have both features (carbon- and oxygen-based) in their spectra (Waters et al. 1998).

The optical properties of the various materials are different and this affects the infrared emission from the dust. The number of planetary nebulae in which the carbon abundance has been estimated is only about 50 (Rola & Stasińska 1994), and even in these objects, it is often very uncertain. Therefore, in our statistical approach, we must take into account the fact that the grain composition varies from object to object in an unknown manner. We have therefore computed models with different grain compositions: graphite (Draine & Laor 1993), amorphous carbon (Rouleau & Martin 1991) and circumstellar silicates (David & Pegourie 1995).

In view of the large parameter space to consider, we have chosen a reference model with $M_* = 0.60\,\mathrm{M}_\odot$, $M_{\rm neb} = 0.2\,\mathrm{M}_\odot$, $v_{\rm exp} = 20\,\mathrm{km\,s^{-1}}$ and dust grains composed of graphite, with $m_{\rm d}/m_{\rm g} = 7.5\,10^{-4}$ (which corresponds to a dust-to-hydrogen mass ratio $m_{\rm d}/m_{\rm H} = 10^{-3}$). In the figures presented below, we discuss differences with respect to this reference model by changing only one defining parameter. In the panels with label a, M_* takes the values 0.58, 0.60, 0.62 and $0.64\,\mathrm{M}_\odot$; in panels b, $M_{\rm neb} = 0.1$, 0.2 and $0.4\,\mathrm{M}_\odot$; in panels c, $v_{\rm exp} = 10$, 20 and $40\,\mathrm{km\,s^{-1}}$; in panels d, $m_{\rm d}/m_{\rm H} = 10^{-4}$, 10^{-3}, 10^{-2} and 10^{-1}; finally, in panels e we explore various dust compositions: graphite, amorphous carbon and circumstellar silicates. It is then relatively easy, from these figures, to imagine the behavior of a model of any arbitrary combination of defining parameters.

All the sequences of models have been computed with a time step of 500 yr, until an age of 10 000 yr was reached, and each symbol in the figures below represents one model. Therefore zones where points accumulate in a theoretical diagram correspond to zones where observational points should accumulate too (if observational selection does not discriminate against this particular zone). It would have been more satisfactory to build the models until a given surface brightness was reached. This, however, would result in very long sequences for some cases, since it is easily shown that the time to reach a given surface brightness goes like $M_{\rm neb}^{2/5} v_{\rm exp}^{-1}$ when the nebulae have reached the optically thin regime.

4. The contamination of IRAS broad band fluxes by line emission in the model nebulae

As discussed in Pottasch et al. (1984a,b) and Lenzuni et al. (1989), the broad band fluxes measured by IRAS are not only due to dust emission. There is a contribution from atomic line emission, as seen directly in the low resolution IRAS spectra of planetary nebulae (see e.g. Pottasch et al. 1984b). Because this effect was especially important in the 12 μm band, Pottasch et al. (1984a) and Lenzuni et al. (1989) were careful not to use fluxes from this band to derive the dust properties (or, rather, they used them only as upper limits). Some later studies, however (Zhang & Kwok 1993, Tajitsu & Tamura 1998) seem to have ignored this problem.

Volk (1992) and Vil'koviskii & Efimov (1992) included the line emission in their model computations of the IRAS fluxes. Volk (1992), for example, showed that the IRAS color-color diagram was strongly affected by atomic line emission, principally in the 12 μm band. However, he explored only a very restricted parameter space, and it is interesting to see how the lines affect the IRAS fluxes in general during the planetary nebula evolution.

Fig. 1a–e shows the ratio F_{12}(d+l)/F_{12}(d) of the total emission in the 12 μm band (d+l stands for dust + lines) and the emission due to dust only (d), as a function of $S(\mathrm{H}\beta)$ for our model planetary nebulae. Figs. 2a–e, 3a–e and 4a–e are equivalent to Fig. 1a–e for F_{25}, F_{60} and F_{100}, respectively.

We see that, as the nebula ages, the line contribution to the F_{12} emission increases. This is because, as the nebula expands, the grains become cooler and gradually emit at longer wavelengths. With the gas chemical composition chosen in our models, the lines that contribute most to the 12 μm band are [Ne II] 12.8 μm, then [S IV] 10.5 μm, [Ar IV] 9.0 μm, [Ar V] 7.9 μm and [Ne V] 14.3 μm. The latter two lines become strong only if the central star is still luminous when it reaches a temperature above 150 000 K, which does not occurs for central stars with $M_* \geq 0.62\,\mathrm{M}_\odot$. Note that [Ne III] 15.5 μm, mentioned by Pottasch et al. (1984a) does not contribute to the 12 μm band. In the most extreme cases, lines may completely dominate the flux in the 12 μm band. Even for relatively young objects, the line contribution may still be important, depending on the charac-

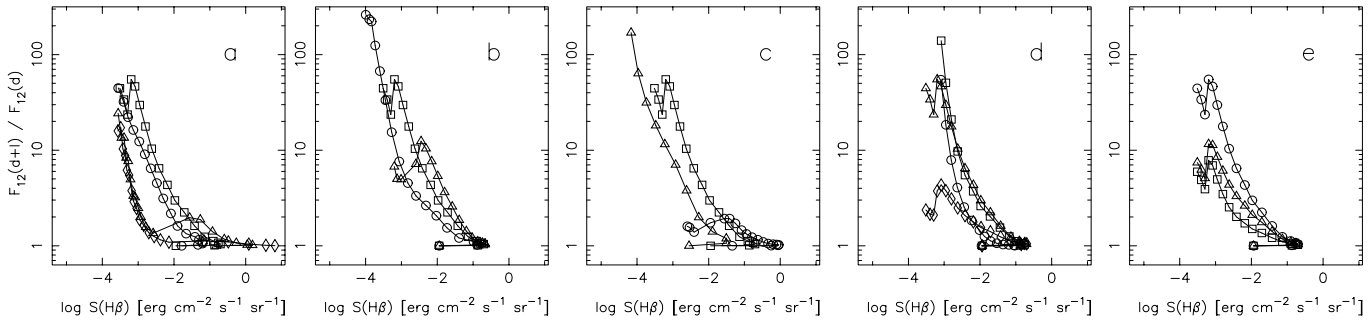

Fig. 1a–e. The ratio F_{12}(d+l)/F_{12}(d) of total emission and pure dust emission in the 12 μm band vs. $S(\mathrm{H}\beta)$ for sequences of models computed at intervals of 500 yr until 10 000 yr. Each panel correspond to the variation of one parameter with respect to the reference model ($M_* = 0.60\,\mathrm{M}_\odot$, $M_{\rm neb} = 0.2\,\mathrm{M}_\odot$, $v_{\rm exp} = 20\,\mathrm{km\,s^{-1}}$ and graphite grains with $m_{\rm d}/m_{\rm g} = 7.5\,10^{-4}$). **a:** stellar mass M_*: $0.58\,\mathrm{M}_\odot$ (circles), $0.60\,\mathrm{M}_\odot$ (squares), $0.62\,\mathrm{M}_\odot$ (triangles), $0.64\,\mathrm{M}_\odot$ (diamonds). **b:** nebular mass $M_{\rm neb}$: $0.1\,\mathrm{M}_\odot$ (circles), $0.2\,\mathrm{M}_\odot$ (squares), $0.4\,\mathrm{M}_\odot$ (triangles). **c:** expansion velocity $v_{\rm exp}$: $10\,\mathrm{km\,s^{-1}}$ (circles), $20\,\mathrm{km\,s^{-1}}$ (squares), $40\,\mathrm{km\,s^{-1}}$ (triangles). **d:** dust content $m_{\rm d}/m_{\rm g}$: $7.5\,10^{-2}$ (circles), $7.5\,10^{-3}$ (squares), $7.5\,10^{-4}$ (triangles), $7.5\,10^{-5}$ (diamonds). **e:** dust material: graphite (circles), amorphous carbon (squares), circumstellar silicates (triangles).

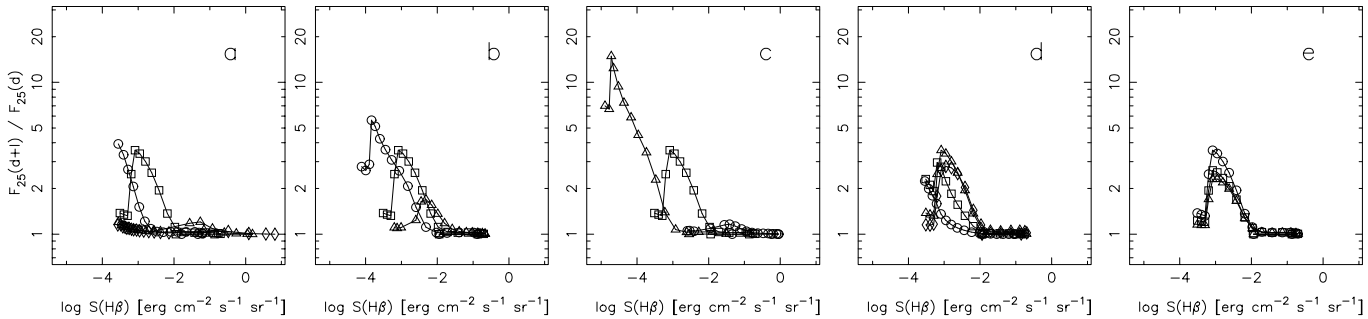

Fig. 2a–e. Same as Fig. 1 but for the ratio F_{25}(d+l)/F_{25}(d)

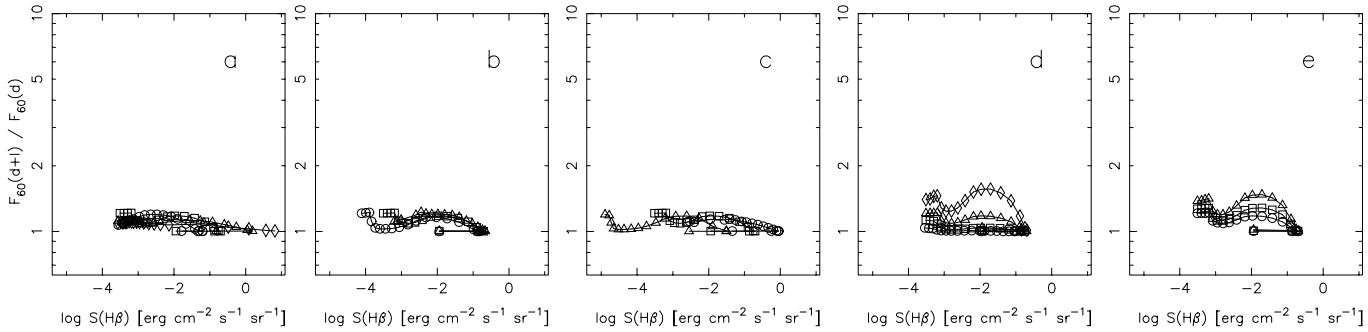

Fig. 3a–e. Same as Fig. 1 but for the ratio F_{60}(d+l)/F_{60}(d)

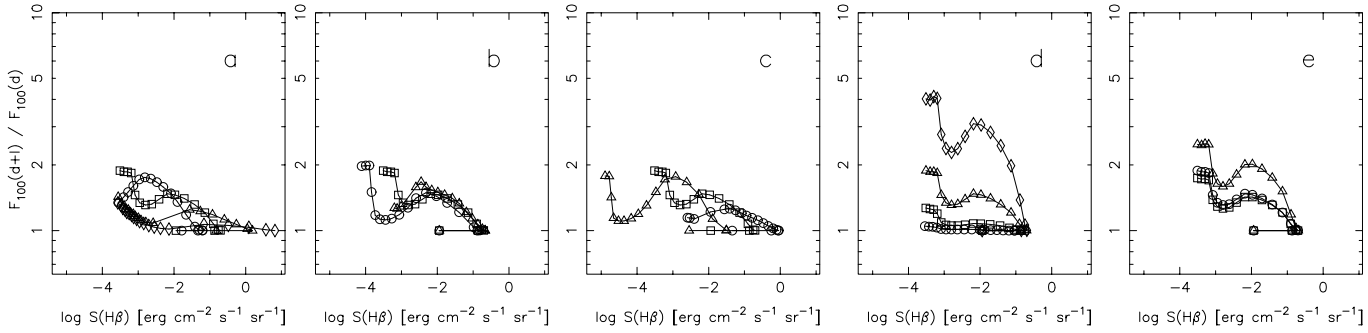

Fig. 4a–e. Same as Fig. 1 but for the ratio F_{100}(d+l)/F_{100}(d)

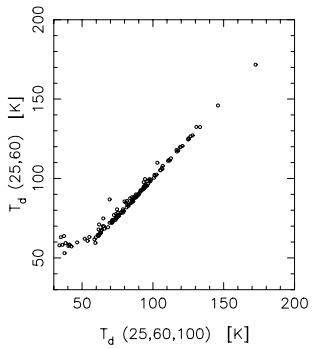

Fig. 5. The color temperature derived from the F_{25}/F_{60} ratio as a function of the temperature derived by a mean square fitting of $\lambda^{-1}\,B_\lambda(T_\mathrm{d})$ to the observed emission in the three bands 25, 60 and 100 μm, giving equal weight to all three fluxes, for our sample of planetary nebulae.

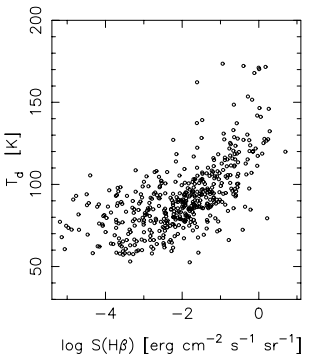

Fig. 6. The color temperature derived from the F_{25}/F_{60} ratio as a function of $S(\mathrm{H}\beta)$ for our sample of planetary nebulae.

teristics of the object and its chemical composition. Therefore, unless a direct estimate of the infrared line strengths is available, one should not use the observed flux in the 12 μm band (except as an upper limit) to infer average dust properties. A further problem with the 12 μm band is that it is contaminated by the emission from the very small grains that experience transient heating which could be especially important in the case of emission by polycyclic aromatic hydrocarbons.

It is interesting to note, in Fig. 1d, that F_{12}(d+l)/F_{12}(d) is the smallest in the sequence of models with the lowest $m_\mathrm{d}/m_\mathrm{g}$. Intuitively, one might expect this ratio to be larger when the amount of dust in a nebula is smaller. What happens, in such a case, is that the total available energy to heat the grains is shared among a smaller number of particles, making each one hotter and the result is a larger dust emission at 12 μm.

In comparison with the F_{12} emission, the line contribution to the F_{25} emission is much smaller, but it can still dominate the dust emission by up to a factor about 3 in the later stages of evolution, as the lines contributing most are [O IV] 25.9 μm and [Ne V] 24.3 μm.

The band with the smallest contribution of atomic lines in our models is the 60 μm one (< 50 % in all cases), with the lines of [O III] 51.8 μm and [N III] 57.3 μm contributing mostly. This band is much wider than the 12 and 25 μm bands, and much of the dust emission in planetary nebulae goes through this band.

The F_{100} emission is not too much affected by line emission ([O III] 88.4 μm and [N II] 121.9 μm being the contributors) except at a very low dust-to-gas mass ratio (of about 10^{-4}, see Fig. 4d). However, it has been reported (IRAS Explanatory Supplement 1988) that the 100 μm band may be contaminated by cirrus emission so that its use for planetary nebulae may be misleading unless a careful analysis of each case is made individually.

5. The dust temperature

Characteristic dust temperatures are generally obtained by fitting the observed spectrum with either $B_\lambda(T_\mathrm{d})$, where T_d is the dust temperature, or a function which approximates the dust emissivity: $\lambda^{-1}\,B_\lambda(T_\mathrm{d})$ or $\lambda^{-2}\,B_\lambda(T_\mathrm{d})$ (e.g. Pottasch et al. 1984a, Iyengar 1986, Zhang & Kwok 1993). In the present study, we use $\lambda^{-1}\,B_\lambda(T_\mathrm{d})$ because such a function better represents the wavelength dependence of grain emissivity for the grains we have chosen.

That such a quantity as a characteristic dust temperature can be defined in a nebula may be surprising. Indeed, there is a distribution of the temperatures of the dust grain particles inside the nebulae. Larger grains have smaller temperatures, since they are heated proportionally to their surface and radiate proportionally to their volume. Also, regions closer to the central star have higher dust temperatures because the stellar radiation field is less diluted. Finally, grains located in the ionized zone of the nebula are heated by a harder radiation field than those located in the neutral zone where only the stellar photons at energies below 13.6 eV and the Lyα photons operate. Nevertheless, our models show that, after integrating over all the grain particles in a given nebula, the resulting infrared spectrum is reasonably indicative of a characteristic dust temperature. The main parameter that affects the dust temperature during the evolution of a model nebula is the average distance of the dust particles from the central star, which varies by a factor 20 between 500 and 10 000 yr.

To determine the characteristic dust temperature in the simplest way one can use the ratio of the infrared fluxes in two bands only, assuming that dust radiates like a single blackbody with an emissivity proportional to λ^{-1}. This is a so-called color temperature. We have tested on our models that the color temperature derived from the F_{25}(d)/F_{60}(d) ratio is very close to the temperature derived by a mean square fitting of $\lambda^{-1}\,B_\lambda(T_\mathrm{d})$ to the pure dust emission in the 25, 60 and 100 μm bands, giving equal weight to all three fluxes (which confirms that the concept of a characteristic dust temperature is indeed a valid one). Similarly, these temperatures are also in agreement in the observed planetary nebulae, as shown in Fig. 5, where the contribution of lines (and cirrus emission in the 100 μm band) adds some slight dispersion. Using a color dust temperature based on 25 and 60 μm fluxes allows us to derive characteristic temperatures in a consistent way for a large sample of planetary nebulae. From now on, T_d will refer to the dust temperature determined in such a way. In principle, one should integrate $\lambda^{-1}\,B_\lambda(T_\mathrm{d})$

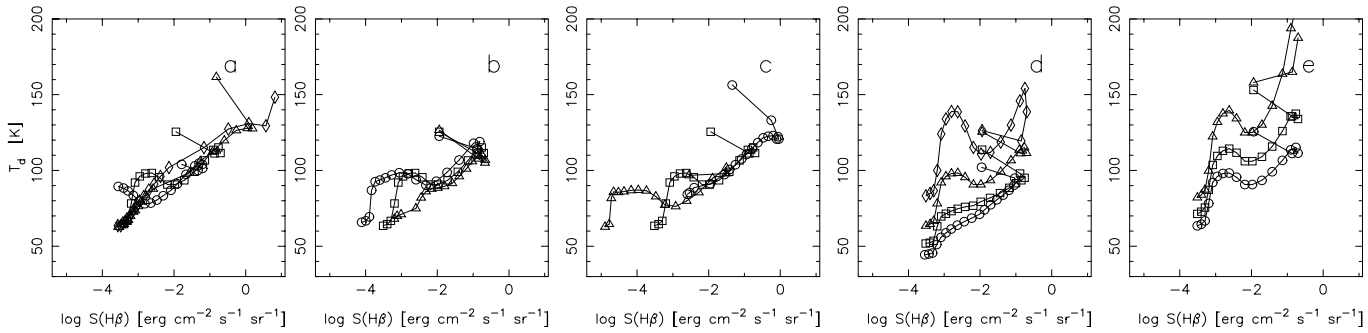

Fig. 7a–e. The color temperature derived from the F_{25}(d+l)/F_{60}(d+l) ratios in the models as a function of $S(\mathrm{H}\beta)$. Same conventions as Fig. 1.

over the IRAS bands but we have checked that doing this results in increasing T_d by less than 10%. Column 6 of Table 1 lists the values of T_d for all the planetary nebulae of our sample.

Fig. 6 shows the values of T_d as a function of the nebular average surface brightness, which has been computed using the reddening corrected Hβ fluxes. There is a clear trend of decreasing T_d with decreasing $S(\mathrm{H}\beta)$. This is reminiscent of the trend found by Pottasch et al. (1984a) and Lenzuni et al. (1989) of the dust temperature decreasing with increasing nebular radius, but the diagram has the advantage of being distance independent. The dust temperatures in Fig. 6 range between 180 K and 50 K. A few objects, namely M 2–23, M 1–48, He 2–34, PC 11, He 2–171, M 2–6 and H 1–36, have T_d higher than 200 K and do not appear in the plot.

Fig. 7a–e shows the same as Fig. 6 for our sequences of model planetary nebulae, the values of T_d being derived from the emission in the 25 and 60 μm bands *including the lines*. Roughly, the models show a trend of decreasing T_d with decreasing surface brightness. This is explained by a decreasing efficiency of the heating, mainly due to a dilution of the stellar radiation field inside the nebula as it expands. The models reproduce the observed diagram remarkably well, given their simplicity. Taking all the models together, one reproduces the observed range in T_d, and the observed variation with $S(\mathrm{H}\beta)$. The increase in T_d at the lowest $S(\mathrm{H}\beta)$ is due to an increasing contribution of the lines to F_{25}, as seen in Fig. 2.

6. The dust-to-gas mass ratio

The formula used by Pottasch et al. (1984a) to derive dust-to-gas mass ratios in planetary nebulae depends on the assumed distance. We prefer using a formula that is distance independent.

The infrared luminosity at the wavelength λ is:

$$4\,\pi\,d^2\,F_\lambda\;=\;\int_{a_\mathrm{min}}^{a_\mathrm{max}}\int_{R_\mathrm{in}}^{R_\mathrm{out}} K_\lambda^\mathrm{abs}(a)\rho_\mathrm{d}(r,a)B_\lambda(T_\mathrm{d}(r,a))(4\,\pi\,r)^2\mathrm{d}r\,\mathrm{d}a \quad (1)$$

where: F_λ is the measured flux from the source at the distance d; a_min and a_max are minimum and maximum dust grain sizes; $K_\lambda^\mathrm{abs}(a)$ is the mass absorption coefficient (which, is almost independent of a at infrared wavelengths); $\rho_\mathrm{d}(r,a)$ is the dust density. So, if $B_\lambda(T_\mathrm{d})$ can be considered uniform in the nebula and independent of a, which, as we checked in our models, is not a bad approximation, then the dust mass is simply given by

$$m_\mathrm{d}\;=\;\frac{F_\lambda d^2}{K_\lambda^\mathrm{abs}B_\lambda(T_\mathrm{d})} \quad (2)$$

The total luminosity in Hβ is approximately given by:

$$4\,\pi\,d^2\,F_{\mathrm{H}\beta}\;=\;\int_{R_\mathrm{in}}^{R_\mathrm{out}} 4.1\,10^{-22}T_\mathrm{e}^{-0.88}n_\mathrm{e}n_{\mathrm{H}^+}4\pi r^2\mathrm{d}r \quad (3)$$

where the emissivity in Hβ is given by Eq. IV–25 of Pottasch (1984); T_e and n_e are the electron temperature and density, respectively; n_{H^+} is the density of ionized hydrogen. If the gas is fully ionized and the density is constant the total gas mass is given by

$$m_\mathrm{g}\;=\;\frac{1.4m_\mathrm{H}4\pi d^2F_{\mathrm{H}\beta}}{4.1\,10^{-22}T_\mathrm{e}^{-0.88}n_\mathrm{e}} \quad (4)$$

where m_H is the mass of the hydrogen atom and the factor 1.4 comes from the classical assumption of a He/H ratio of 0.1. For simplicity, we will assume for the remaining of the paper that $T_\mathrm{e}=10^4$ K.

Therefore, using Eqs. (2) and (4) the dust-to-gas mass ratio is given by

$$m_\mathrm{d}/m_\mathrm{g}\;=\;\frac{F_\lambda}{F_{\mathrm{H}\beta}}\frac{1}{K_\lambda^\mathrm{abs}B_\lambda(T_\mathrm{d})}\frac{4.1\,10^{-22}T_\mathrm{e}^{-0.88}n_\mathrm{e}}{1.4m_\mathrm{H}4\pi} \quad (5)$$

In principle, if the colour temperature is used, one can use equally well the fluxes in the 25 μm or the 60 μm band to estimate $m_\mathrm{d}/m_\mathrm{g}$. However, since atomic lines may contribute to the observed IRAS fluxes, we prefer to show results based on the 60 μm fluxes, since this band is less contaminated, as seen above (but the overall appearance of the diagrams based on the 25 μm fluxes is very similar to the ones presented in this paper).

To check the method before applying it to observed nebulae, we use it on our models, where we know the input dust properties and dust-to-gas mass ratio. Fig. 8a–e shows the values of $m_\mathrm{d}/m_\mathrm{g}$ as derived from Eq. (5), as a function of $S(\mathrm{H}\beta)$ for our different series of models. In each case, we take the value of K_{60}^abs that corresponds *exactly* to the one used in the model: 145.32 cm^2 g^{-1} for graphite, 74.38 for amorphous carbon and 53.45 for circumstellar silicates.

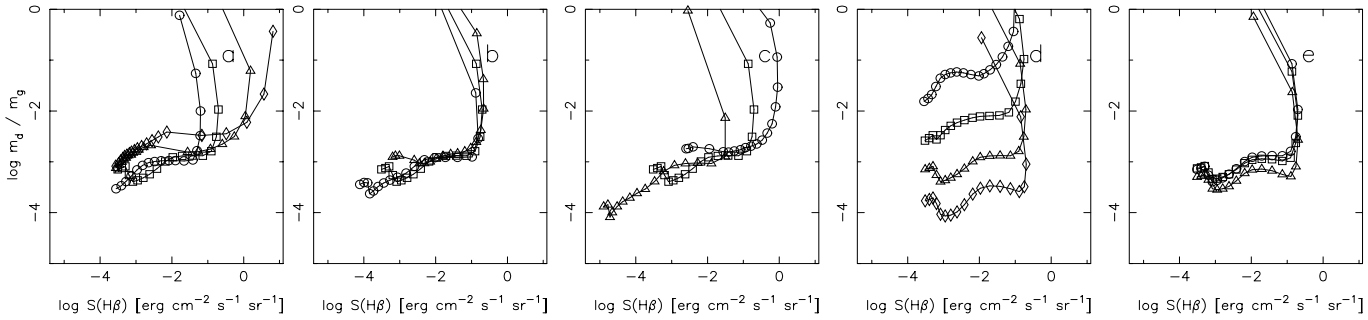

Fig. 8a–e. The values of $m_{\rm d}/m_{\rm g}$ derived from Eq. (5) for the models as a function of $S(\rm H\beta)$. Same conventions as Fig. 1.

We find that, for many of the models, the formula returns an estimated dust-to-gas mass ratio within $\pm\,0.3$ dex of the input one. Of course, the models that are optically thick return $m_{\rm d}/m_{\rm g}$ values larger than the input ones, since the Hβ flux corresponds to the ionized region only. Most of those optically thick models correspond to the vertical tracks seen in Fig. 8 a–e, at the beginning of the planetary nebulae evolution. As seen in this figure, the total number of model points on these vertical tracks is small compared to the number of points in the later stages and they are located on the high surface brightness side of the diagram. Indeed, it can be shown that, whithin the theoretical framework adopted here, planetary nebulae with $M_* \leq 0.62\,{\rm M}_\odot$ are in an ionization bounded stage only during a short fraction of their observable lifetime, irrespective of the nebular mass and expansion velocity. For planetary nebule whose central stars have higher masses, however, the proportion of time spent in the ionization bounded regime is larger (see the figures in Stasińska et al. 1998), due to the fact that the stellar luminosity drop occurs early in the lifetime of the planetary nebula; the model with $M_* = 0.64\,{\rm M}_\odot$ in Fig. 8a, corresponds to such a case. There are however evidences that the total number of planetary nebulae with central stars more massive than $0.62\,{\rm M}_\odot$ is not large, 20% at the very most (see Stasińska et al. 1997). We note also, in Fig. 8, and especially in panels a–c, that, for some of the very low surface-brightness models, the use of Eq. (5) underestimates the dust-to-gas mass ratio. These cases correspond to phases where the atomic line contribution to the 25 μm flux is important, as seen in Fig. 2a–e, so that the colour temperature of the dust is overestimated which induces an underestimation of the dust-to-gas mass ratio. In our series of models, this effect is really strong only in a few cases, mostly at the low surface brightness end. However, the effect will be larger at higher metallicities than considered in the models presented here.

It is interesting to compare the range in the derived $m_{\rm d}/m_{\rm g}$ values with the range of the input values of $m_{\rm d}/m_{\rm g}$ in our series of models. Fig. 8d shows that, if one excepts the optically thick cases, the method tends to narrow the $m_{\rm d}/m_{\rm g}$ range with respect to the input one at a given $S(\rm H\beta)$. This results from contamination of the IRAS bands by atomic lines, as can be understood by considering Figs. 2 and 3. With larger abundances of the metals than in our models, the effect would be even more pronounced. This means that the method itself, when applied to real nebulae, does not artificially widen the distribution of dust-to-gas mass ratios with respect to $S(\rm H\beta)$.

The sequence of models computed with circumstellar silicates systematically returns a smaller dust-to-gas mass ratio than the series computed with graphite or amorphous carbon grains (Fig. 8e). This is because in our determination of $T_{\rm d}$, we assumed that the dust emissivity varies like λ^{-1}, which is indeed the case when comparing the 25 and 60 μm wavelengths for graphite and amorphous carbon, while for circumstellar silicates the true dependence is rather like λ^{-2}. Therefore, we overestimate the dust temperature, and, consequently underestimate the dust mass. This effect is not very strong, about a factor 2 in $m_{\rm d}/m_{\rm g}$. However if we determine the dust-to-gas mass ratio of the model containing silicates using the value of $K_{60}^{\rm abs}$ for graphite, simulating the analysis of an object for which we do not know the true value of $K_{60}^{\rm abs}$, the estimated dust-to-gas mass ratio goes down by an additional factor of about 2.

In summary, combining all the uncertainties, the method to determine the dust-to-gas mass ratio should give estimates within, let us say, $\pm\,0.3$ dex in the majority of planetary nebulae. As is known, it overestimates $m_{\rm d}/m_{\rm g}$ in the case of planetary nebulae that are incompletely ionized. Our models show that such cases, however, should represent a small fraction of observed nebulae, unless one is dealing with samples at high surface brightness. On the other hand, there is probably a tendency to underestimate the dust-to-gas mass ratio for low surface brightness objects, due to contamination of the IRAS fluxes by atomic lines, even when selecting the best IRAS bands, as we have done here.

We now turn to the observational sample. Using Eq. (5), where $F_{\rm H\beta}$ now represents the reddening corrected nebular flux in Hβ and taking for $K_{60}^{\rm abs}$ the value of $145.3\,{\rm cm}^2\,{\rm g}^{-1}$ corresponding to graphite grains, we have computed the values $m_{\rm d}/m_{\rm g}$ for our sample of planetary nebulae from the observed fluxes in the 60 μm band. These $m_{\rm d}/m_{\rm g}$ are reported in Column 7 of Table 1. Fig. 9 shows $m_{\rm d}/m_{\rm g}$ as a function of $S(\rm H\beta)$. We find that in 70% of the cases the estimated values of $m_{\rm d}/m_{\rm g}$ lie between 10^{-2} and 10^{-3}, in 15% of them they are larger than 10^{-2} and in 15% of them they are smaller than 10^{-3}, the extremes being close to 10^{-1} and 10^{-4}. Accounting for the fact that some planetary nebulae in the sample are ionization bounded, and that atomic line contribution may result in an underestimation of $m_{\rm d}/m_{\rm g}$ in some low surface brightness

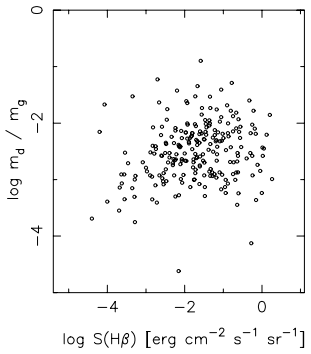

Fig. 9. The dust-to-gas ratio derived from Eq. (5) as a function of $S(\mathrm{H}\beta)$ for our sample of planetary nebulae.

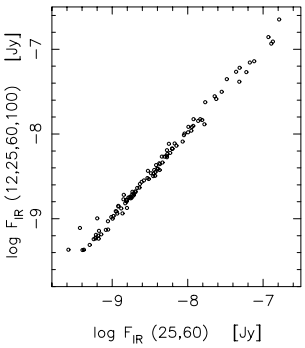

Fig. 10. The total infrared flux estimated from the IRAS fluxes at 12, 25, 60 and 100 μm as a function of the total infrared flux estimated from the IRAS fluxes at 25 and 60 μm only

objects, the true range in $m_\mathrm{d}/m_\mathrm{g}$ is probably of about a factor 10. As a consequence, the dust-to-gas mass ratio is a primordial parameter for the interpretation of far infrared data of planetary nebulae. This was not always taken into account in former studies of statistical nature (Volk 1992, Zhang & Kwok 1993, Tajitsu & Tamura 1998).

Clearly, in Fig. 9 there is no correlation between $m_\mathrm{d}/m_\mathrm{g}$ and $S(\mathrm{H}\beta)$ (the Pearson correlation coefficient is 0.132 for 230 points, with an associated probability of 0.05). Objects with very low or very high $m_\mathrm{d}/m_\mathrm{g}$ are found at any $S(\mathrm{H}\beta)$. The systematic errors in the determination of $m_\mathrm{d}/m_\mathrm{g}$ that were discussed above would tend to overestimate $m_\mathrm{d}/m_\mathrm{g}$ at high $S(\mathrm{H}\beta)$ and underestimate it at low $S(\mathrm{H}\beta)$. But, as we have argued above, important errors are not likely to affect a large fraction of the sample. We conclude that there is no evidence for a decrease in the dust-to-gas mass ratio as the planetary nebulae evolve.

7. The total infrared flux and the infrared excess

Several papers have studied the total infrared flux and infrared excess in planetary nebulae. Pottasch et al. (1984a) noted that younger planetary nebulae have higher IRE. Ratag et al. (1990) compared a sample of about 100 planetary nebulae in the galactic bulge and a sample of about 100 bright nearby nebulae, and found that the latter showed, on average, lower IRE. They advocated that one possibility could be for example that, because of selection effects, planetary nebulae from the bulge sample would be, on average, of higher surface brightness and thus, younger. Another possibility suggested by Zijlstra et al. (1989) is that the higher IRE in the bulge planetary nebulae could be due to a higher dust content, related to a higher metallicity in the bulge. However, Ratag et al. (1990) rejected this option since the average metallicity of the bulge planetary nebulae is not that much different from the average metallicity of nearby disk planetary nebulae. They then argued that the bulge planetary nebulae, being descendent of a lower mass stellar population, would have lower mass nuclei. These would spend a longer time at lower effective temperature, inducing higher IRE due to the larger contribution of stellar non ionizing photons to the dust heating. Finally, they explored the possibility that the high IRE in the galactic bulge planetary nebulae could be due to additional dust heating by the interstellar radiation field. They estimated that, for a planetary nebula located in the galactic bulge, an energy of 100 to 400 $\mathrm{L}_\odot$ would be provided by the interstellar radiation field.

Our models are able to provide some insight into these questions, but let us first discuss the empirical determination of the total infrared flux.

The total radiation that is emitted by dust in a nebula can be estimated from the IRAS fluxes basically by two methods. One is simply to compute the flux under the curve defined by the observed infrared fluxes, as done by Pottasch et al. (1984a). The other is to fit the observed energy distribution by a function proportional to $\lambda^{-1}\,B_\lambda(T_\mathrm{d})$. The simplest version of this method is to compute the blackbody flux that corresponds to the ratios of the observed fluxes at 25 and 60 μm. Beside the advantage of being computationally simple, this method allows one to consider a large number of planetary nebulae, since it requires fluxes in only two bands, and it is the least affected by atomic line and cirrus emission. It is interesting to compare the results of these two methods. This is done in Fig. 10 where we plot the total IRAS flux determined by the first method using the fluxes at 12, 25, 60 and 100 μm as a function of the total IRAS flux derived by the simplest version of the second method. In building this diagram, we considered only those objects with $Q = 3$ in the four IRAS bands, so that the total number of objects represented is only 107. The observed correlation is very good over the whole range of fluxes. From this, we feel confident that we can indeed use only the 25 and 60 μm fluxes to estimate the total infrared flux. The infrared excess is then determined from the total infrared flux and the total reddening corrected Hβ flux using

$$\mathrm{IRE} = \frac{F_\mathrm{IR}}{23.3\,F_{\mathrm{H}\beta}} \qquad (6)$$

where 23.3 is the ratio of Lyα to Hβ emission (Table VIII-2 of Pottasch 1984).

Fig. 11 shows the IRE, determined in such a way, as a function of the angular distance to the Galactic center for our sample of planetary nebulae. The sample is much larger than considered in previous studies since it contains more than 500 objects. There is indeed a tendency for the average infrared excess to decrease

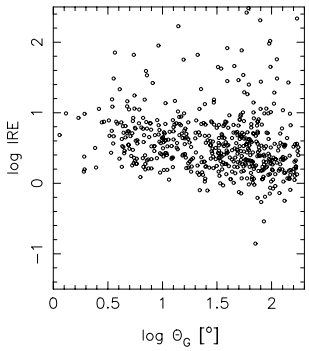

Fig. 11. The values of IRE derived from Eq. (6) as a function of the angular distance to the Galactic center for our sample of planetary nebulae.

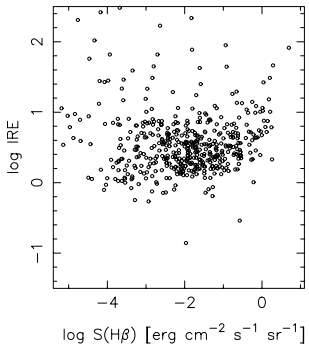

Fig. 12. The values of IRE derived from Eq. (6) as a function of $S(\mathrm{H}\beta)$ for our sample of planetary nebulae.

with increasing angular distance to the Galactic center. However, the variation is not exactly the one that would be expected if the interstellar radiation field alone were to produce this effect, as suggested by Ratag et al. (1990) and Amnuel (1994). Indeed, the variation is very smooth and shows no marked peak in the direction of the bulge. We also note the existence of objects (about 10% of the whole sample) with IRE > 10, and those are distributed uniformly in Galactic longitude. This indicates that these high IRE are related to an intrinsic property of the nebulae and not to their location in the Galaxy.

Fig. 12 shows the IRE as a function of $S(\mathrm{H}\beta)$. In this figure, which contains over 470 points (the angular diameter is required in addition to the Hβ flux), one can see that planetary nebulae of high or low surface brightness can have equally high IRE. There is no evidence that the IRE is higher for the younger nebulae.

Fig. 13a–e represents the same diagram as Fig. 12 for our sequences of models. It shows that, for the earliest evolutionary stages, when the central star does not emit a large proportion of ionizing photons, the infrared excess can indeed reach very high values, as was argued in several previous studies. But, according to our models, such optically thick objects should be rare. On the other hand, large values of the IRE are easily produced when $m_{\mathrm{d}}/m_{\mathrm{g}}$ is high (Fig. 13d). Since we have shown that large dust-to-gas ratios occur for planetary nebulae of all ages, the same is true for large values of the IRE.

It has been suggested by Zijlstra et al. (1989) that the infrared excess may be used as a measure of the temperature of the central stars, T_{eff}, for stars cooler than 40 000 K (for larger values of T_{eff}, the proposed calibration becomes multivalued). Fig. 14a–e shows the IRE as a function of T_{eff} in our sequences of models. From this figure, we see that the method is less reliable than it appears from Fig. B1 of Zijlstra et al. (1989). Even for the coolest stars, for a given T_{eff}, the IRE depends somewhat on the mass of the central star, on the nebular mass and expansion velocity and, most importantly, on the dust-to-gas mass ratio. As a result, the derivation of T_{eff} using the infrared excess is not accurate. It will be especially misleading if the dust-to-gas mass ratio in a given nebula does not allow the simplifying assumptions made by Ziljstra et al. (1989) to be valid.

8. The grain size

Lenzuni et al. (1989) estimated the typical size of the dust grains in their sample from the thermal balance equation, under the assumption that the absorption efficiency Q_{UV} was 1 in the UV and that they could estimate the total luminosity of the central star. They found that the average size of the grains, $\overline{a}$, was decreasing from about $3.\,10^{-5}$ cm to $3.\,10^{-8}$ cm as the radius of the nebulae increased from $3.\,10^{16}$ to $1.\,10^{18}$ cm. This was an appealing conclusion, which, combined with their finding that the total dust-to-gas mass ratio was decreasing with time, led to some interesting speculations about the destruction process of dust grains in planetary nebulae.

Actually, it is not quite true that Q_{UV} is constant, it varies strongly with wavelength for grains smaller than about 10^{-6} – $5.\,10^{-6}$ cm depending on the dust material.

The method of Lenzuni et al. (1989) can easily be tested on our models, which all have the same distribution of grain sizes during the whole nebular evolution. The formula they used can be rewritten as:

$$\overline{a} \;=\; \frac{3\,\lambda^{-1}\,Q_{\mathrm{UV}}\,L_*}{(4\,\pi\,r)^2\,4\,\rho_{\mathrm{d}}^{\mathrm{bulk}} K_\lambda^{\mathrm{abs}} \int_0^\infty \lambda^{-1} B_\lambda(T_{\mathrm{d}})\mathrm{d}\lambda} \qquad (7)$$

where L_* is the stellar luminosity and $\rho_{\mathrm{d}}^{\mathrm{bulk}}$ the density of the grain material. In the case of our models, we know the total stellar luminosity, so the formula can be applied easily. Fig. 15a–e shows the resulting value of $\overline{a}$ obtained using Eq. (7) at $\lambda = 60\,\mu$m for our sequences of models. We see that the method to derive $\overline{a}$ is strongly biased, and gives decreasing values of $\overline{a}$ as $S(\mathrm{H}\beta)$ decreases. The effect is quite large: the estimated $\overline{a}$ decrease by about 2 dex as $S(\mathrm{H}\beta)$ decreases by about 4 dex which, in our models, correspond roughly to an increase of the radius by about 1 dex. Therefore, the bias in the method is of the same order of magnitude as the effect found by Lenzuni et al. (1989).

We have not questioned here the way in which Lenzuni et al. (1989) determined L_*. They used an analytical model of HII regions (Panagia 1974) to do this. This model involves many assumptions that are not necessarily fulfilled and might produce an additional bias in one way or another.

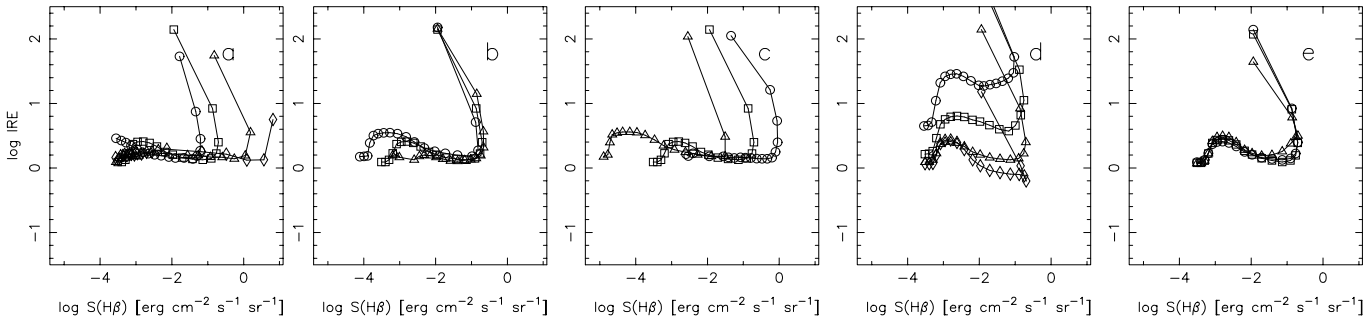

Fig. 13a–e. The values of IRE derived from Eq. (6) for the models as a function of $S(\mathrm{H}\beta)$. Same conventions as Fig. 1.

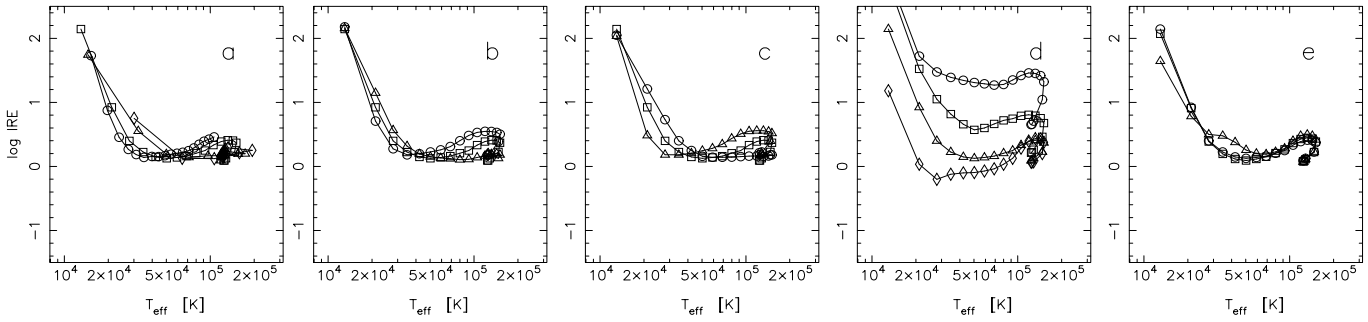

Fig. 14a–e. The values of IRE derived from Eq. (6) for the models as a function of $T_{\rm eff}$. Same conventions as Fig. 1.

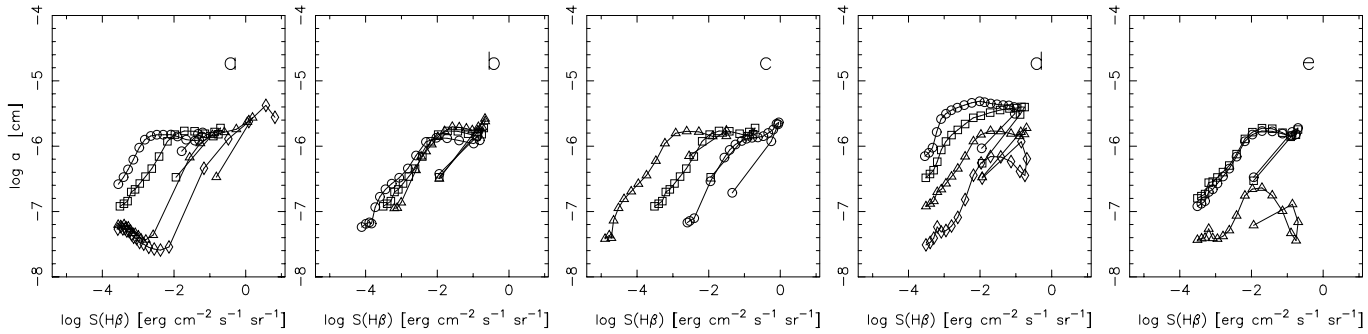

Fig. 15a–e. The values of the average grain size $\overline{a}$ derived from Eq. (7) for the models as a function of $S(\mathrm{H}\beta)$. Same conventions as Fig. 1.

Since, in our models, the value of $\overline{a}$ is $3.53\,10^{-6}$ cm, we see from Fig. 15 that the method of Lenzuni et al. rather tends to underestimate $\overline{a}$. If we consider that the highest values of $\overline{a}$ found by Lenzuni et al. are $\simeq 3.\,10^{-5}$ cm, it might be that indeed such large grains are found in planetary nebulae. Such a conclusion, however, might not be robust, since we have not tested how it would vary if we assumed different size distributions or forms of the grains. Interestingly, we note that, in the Red Rectangle nebula, Jura (1997) has argued, on other grounds, that grains have a large size.

The main conclusion from testing Eq. (7) on our models is that, clearly, one cannot derive the value of $\overline{a}$ in such a way. One could, perhaps estimate this parameter from a detailed model fitting of individual, well observed, objects, but this is not certain and has never been attempted so far to our knowledge. For the time being, we consider that there is no evidence that the typical grain size of dust varies during the evolution of planetary nebulae.

9. Discussion

We have reconsidered the dust content of planetary nebulae by performing a new statistical study of broad band IRAS data. The main difference with previous studies is that our method of analysis was tested on a wide grid of photoionization models of evolving dusty planetary nebulae. Furthermore, our results are based on distance independent diagrams. We are aware that our analysis, although more elaborated than previous studies of statistical nature, still suffers from uncertainties. Detailed modelling of individual objects should, in principle, provide better estimates of the dust content of planetary nebulae. Such an approach is however not feasible on a large sample of objects.

Our main result is that the range in dust-to-gas mass ratios among planetary nebulae is large, about a factor 10, but, in contrast with previous authors, we find no evidence for a change in the dust-to-gas mass ratio in the course of planetary nebu-

lae evolution. Neither do we find evidence for a change in the average grain size.

To our knowledge, the problem of dust survival in planetary nebulae is still poorly understood from a theoretical point of view. The main processes of dust destruction have been described by Draine & Salpeter (1979 and references therein) or Draine (1990) but the estimated efficiencies are uncertain and need confirmation by observation. After the works of Pottasch et al. (1984a) and Lenzuni et al. (1989) the idea that dust is gradually destroyed – by the energetic photons emitted by the central star or by other mechanisms – made its way among astronomers (e.g. Furton & Witt 1992, Dinerstein et al. 1995, Corradi & Schwarz 1995). Our analysis does not support such a view. In addition, there is now observational evidence that dust destruction in planetary nebulae is probably not as strong as thought before. Namely, Volk et al. (1997) have reported that their attempt to search for lines of Ca in planetary nebulae has failed, indicating that Ca is probably locked in grains (see the classical work of Field 1974 which discusses the problem of the gas-phase element depletions) and the UV radiation does not seem to be so efficient for dust destruction. It has been shown by the theoretical calculations of Okorokov et al. (1985) and Marten et al. (1993) that radiation pressure on dust particles accelerates particles to higher velocities and gradually expells them from the nebula. It seems however, that the conclusion of Okorokov et al. (1985) that dust is removed from planetary nebulae almost entirely is too far going. They did not consider the process of charging of the dust particles which probably freezes them into the ionized gas. It is worth of noting, however, that the spread of the points representing the dust-to-gas mass ratio is quite wide and shows that planetary with different dust contents exist. The reason could be at least twofold: planetary nebulae could be created with different dust-to-gas mass ratios on the AGB; or the time spent by the star during the pre-planetary phase of evolution, when the process of dust acceleration and removing is efficient, was different (shorter for planetary nebulae with presently higher dust-to-gas mass ratio). If the second scenario applies, one can speculate that, at least from a statistical point of view, planetary nebulae with smaller dust-to-gas ratio might have less massive central stars.

Acknowledgements. We thank S. Górny for having made available his compilation of electron densities in planetary nebulae and J. Mathis for his precious comments about the manuscript. Remarks by an anonymous referee were helpful in clarifying some aspects of this work. This work is in part supported by the grant 2.P03D.002.13 to R.S. from the Polish State Committee for Scientific Research, by CNRS: "jumelage France–Pologne", by the University Paris 7 and by the Observatoire de Paris-Meudon.

References

Acker A., Jasniewicz G., Köppen J., et al., 1989, A&AS 80, 201
Acker A., Raytchev B., Stenholm B., et al., 1991, A&AS 89, 237
Acker A., Ochsenbein F., Stenholm B., et al., 1992, Strasbourg–ESO Catalogue of Galactic Planetary Nebulae
Adams T.F., 1975, ApJ 201, 350
Amnuel P.R., 1994, Ap&SS 219, 117
Blöcker Th., 1995, A&A 299, 755
Corradi R.L.M., Schwarz H.E., 1995, A&A 293, 871
Daub C.T., 1982, ApJ 260, 612
David P., Pegourie B., 1995, A&A 293, 833
Dinerstein H.L., Sneden C., Uglum J., 1995, ApJ 447, 262
Draine B.T., 1990, In: Bonetti A., Greenberg J.M., Aiello S. (eds.) Evolution of Interstellar Dust and Related Topics. Proceedings of the International School of Physics "Enrico Fermi" Course, North Holland, Amsterdam, New York, p. 103
Draine B.T., Laor A., 1993, ApJ 402, 441
Draine B.T., Salpeter E.E., 1979, ApJ 231, 438
Field G.B., 1974, ApJ 187, 453
Furton D.G., Witt A.N., 1992, ApJ 386, 587
Frank A., Mellema G., 1994, A&A 289, 937
Gęsicki K., Acker A., Szczerba R., 1996, A&A 309, 907
Górny S.K., Stasińska G., Tylenda R., 1997, A&A 318, 256
Harrington J.P., Monk D.J., Clegg R.E.S., 1988, MNRAS 231, 577
Hoare M.G., 1990, MNRAS 244, 193
IRAS Explanatory Supplement, Version 2, 1988, Beichman C.A., Neugebauer G., Habing H., et al. (eds.), NASA Ref. Publ., 1190
IRAS Point Source Catalog, 1988, Joint IRAS Science Working Group, Washington, DC, US GPO
Iyengar K.V.K., 1986, A&A 158, 89
Jura M., Turner J., Balm S.P., 1997, ApJ 474, 741
Kingsburgh R.L., Barlow M.J., 1994, MNRAS 271, 257
Lenzuni P., Natta A., Panagia N., 1989, ApJ 345, 306
Marten H., Szczerba R., Blöcker Th., 1993, In: Planetary Nebulae. Proceedings of the IAU Symp. 155, p. 363
Mathis J.S., Rumpl W., Nordsieck K.H., 1977, ApJ 217, 425
Moseley H., 1980, ApJ 238, 892
Natta A., Panagia N., 1981, ApJ 248, 189
Okorokov V.A., Shustov B.M., Tutukov A.V., et al., 1985, A&A 142, 441
Panagia N., 1974, ApJ 192, 221
Pottasch S.R., 1984, Planetary Nebulae. D. Reidel Publishing Company
Pottasch S.R., Baud B., Beintema D., et al., 1984a, A&A 138, 10
Pottasch S.R., Beintema D., Raimond E., et al., 1984b, ApJ 278, L33
Pottasch S.R., 1987, In: Kwok S., Pottasch S.R. (eds.) Late Satges of Stellar Evolution. Reidel Publishing Company, p. 355
Ratag M.A., Pottasch S.R., Zijlstra A.A., et al., 1990, A&A 233, 181
Rola C., Stasińska G., 1994, A&A 282, 199
Rouleau F., Martin P.G., 1991, ApJ 377, 526
Sabbadin F., 1986, A&AS 64, 579
Stanghellini L., Kaler J.B., 1989, ApJ 348, 811
Stasińska G., Leitherer C., 1996, A&AS 189, 971
Stasińska G., Górny S., Tylenda R., 1997, A&A 327, 736
Stasińska G., Richer M.G., McCall M.L., 1998, A&A 336, 667
Tajitsu A., Tamura S., 1998, AJ 115, 1989
Tylenda R., Stasińska G., 1994, A&A 288, 897
Volk K., 1992, ApJS 80, 347
Volk K., Dinerstein H., Sneden C., 1997, In: Planetary Nebulae. Proceedings of the IAU Symp. 180, p. 284
Vil'koviskii E.Ya., Efimov S.N., 1992, AZh 69, 793
Waters L.B.F.M., Beintema D.A., Zijlstra A.A., et al., 1998, A&A 331, L61
Zhang C.Y., Kwok S., 1993, ApJS 88, 137
Zijlstra A.A., te Lintel Hekkert P., Pottasch S.R., et al., 1989, A&A 217, 157